



Initial experience with dual-energy computed tomography-guided bone biopsies of bone lesions that are occult on monoenergetic CT

Michael C. Burke¹ · Ankur Garg¹ · Jonathan M. Youngner¹ · Swati D. Deshmukh¹ · Imran M. Omar¹

Received: 18 July 2018 / Revised: 24 September 2018 / Accepted: 1 October 2018 / Published online: 20 October 2018
© ISS 2018

Abstract

Objective Our purpose was to determine whether dual-energy CT (DECT), specifically the bone marrow setting of the virtual noncalcium (VNCa) algorithm, could be used to identify and accurately biopsy suspected bone malignancies that were visible on magnetic resonance imaging (MRI), nuclear bone scintigraphy, or positron-emission tomography/computed tomography (PET/CT), but occult on monoenergetic computed tomography (CT) by virtue of being either isodense or nearly isodense to surrounding normal bone.

Materials and Methods We present 4 cases in which DECT was used to detect various malignant bone lesions and was successfully used to direct percutaneous DECT-guided bone biopsies.

Results Two of the lesions were solid tumor metastases (breast and prostate carcinoma), whereas two others were hematological malignancies (leukemia and lymphoma). This technique enabled us to confidently and accurately direct the biopsy needle into the target lesion.

Conclusion The authors demonstrate that the DECT VNCa bone marrow algorithm may be helpful in identifying isodense bone lesions of various histologies and may be used to guide percutaneous bone biopsies. This technique may help to maximize diagnostic yield, minimize the number of passes into the region of concern, and prevent patients from undergoing repeat biopsy.

Keywords Dual-energy CT · Bone biopsy · Isodense bone lesion

Introduction

Dual-energy computed tomography (DECT) has been increasingly used in musculoskeletal imaging for applications ranging from detecting urate deposits in gout, assessing for bone marrow edema and osteoporosis, determining body composition, characterizing tendons and ligaments, and aiding the reduction of metallic artifact [1–12]. This technique allows for discrimination of materials such as calcium, iron, urate and iodine, based on their inherent atomic numbers [13], and these materials can be displayed on CT images with color or grayscale-coded maps, which can help virtually accentuate or eliminate them. Bone marrow assessment on DECT may also be helpful in distinguishing osseous lesions from adjacent normal bone [14].

Most lesions of cortical and medullary bone are well-seen on computed tomography (CT) based on the fact that they are either sclerotic (denser than the adjacent bone) or lucent (less dense than the adjacent bone), and the use of CT-guidance for directing bone biopsies is well established. As a result, the outcomes of percutaneous CT-guided biopsy of bone lesions, including diagnostic yield, diagnostic accuracy, and false-negative rates, have been reported by many groups. However, the reported ranges of these outcomes have been highly variable, with diagnostic yield ranging between 49 and 98%, accuracy between 86 and 97%, and false-negative rates from 2 to 8% [15–28]. In our practice, we are increasingly asked to biopsy lesions that are clearly discernible on magnetic resonance imaging (MRI), nuclear bone scintigraphy, or positron-emission tomography/CT (PET/CT), but appear isodense or nearly isodense to bone on monoenergetic CT. We suspect that this scenario is also encountered at other institutions given the increased volume of medical imaging over the last decade, and may contribute to poor diagnostic yield and false-negative biopsy. Other authors have recommended various strategies for lesion localization in this setting, including use of a

✉ Michael C. Burke
michael.c.burke.85@gmail.com

¹ Department of Radiology, Northwestern University Feinberg School of Medicine, 676 North Saint Clair Street, Suite 800, Chicago, IL 60611, USA

previous MRI as an anatomical road map during the CT-guided biopsy [29], direct MRI-guided bone biopsy [30, 31] or using PET/CT during the biopsy to guide needle trajectory [32, 33]. However, MRI road mapping can lead to sampling error and false-negative biopsies; MRI-guided bone biopsies require specialized biopsy devices and often result in large artifacts that may prevent visualization of the lesion as the needle is advanced in to the bone; and PET/CT-guided biopsies, particularly the PET portion of the study, may result in added time and expense.

A number of authors have discussed the potential use of DECT in detecting bone neoplasms. There have been a few recent reports discussing its use in both hematogenous malignancies, such as multiple myeloma [34–36], and solid bone neoplasms, such as metastases [37–42]. The goal of this article is to describe our initial experience using DECT to improve bone lesion visualization, and utilization of these images to aid CT-guided biopsy to potentially decrease sampling error.

Materials and methods

Patient selection

This retrospective study was granted an internal review board waiver and consisted of four consecutive patients with a history of primary malignancy. The study consisted of four patients with bone lesions identified on contrast-enhanced MRI and/or PET/CT that were either not discernable or not easily discernable on subsequent monoenergetic CT or the attenuation correction CT images from PET/CT. Although no patients were excluded based on other criteria, the lesions needed to be amenable to safe percutaneous access and the patients needed to be able to tolerate the procedure, including optimal positioning without significant movement to allow the maintenance of a safe, sterile field. Additionally, patients were pre-screened for a history of bleeding diathesis, anticoagulant use, or active infection. No other patients were considered for the study, and the four patients represented our total experience with this technique to date.

Dual-energy CT protocol

Unenhanced CT examinations were performed using a third-generation dual-source dual-energy CT system (Somatom Force; Siemens, Forchheim, Germany). The two X-ray tubes were operated at different kilovolt settings (tube A: 90 kVp, 245 mAs; tube B: Sn150 kVp [0.64 mm tin filter], 350 mAs). All of the patients in our study weighed less than 90 kg. However, if any patient had weighed more than 90 kg, the kilovolt setting on tube A would have been increased to 100 kVp. Axial CT was performed in the craniocaudal direction with a dual-energy protocol (rotation time, 0.5 s; pitch 0.5;

collimation, 128 × 0.6 mm). Automatic attenuation-based tube current modulation (CASE dose 4D; Siemens Healthineers) was utilized. Mean volume CT dose index was 18.37 mGy (range, 3.0–13.3 mGy) and mean dose-length product was 339 mGy/cm (range, 86.6–789.1 mGy/cm).

Post-processing was performed on dedicated dual-energy software (Syngo.via; version VA30; Siemens Healthineers) with a three-material decomposition algorithm for bone mineral, yellow marrow, and red marrow, based on the following material definitions (which represent the default settings): calcium slope: 1.65; yellow marrow, –108/–84 HU (low/high kV tube); red marrow, 52/51 HU for the 90/150 kV setting. The parameters in the 100/150 kV setting were set to a calcium slope: 1.53; yellow marrow: –105/–84 HU; red marrow: 52/51 HU. For further assessment, DECT images were viewed as weighted average CT fused with a virtual noncalcium (VNCa) color map overlay using the bone marrow setting (Siemens Healthineers).

Bone biopsy technique

Initial pre-procedural imaging, either MRI or PET/CT, was used to plan the optimal pathway for percutaneous access to each lesion. The patient was placed on the CT table and an initial DECT was performed. Grayscale imaging was viewed in the bone window to assess for areas of osteolysis or aggressive periosteal reaction in the area of concern, and in the soft-tissue window to detect areas of altered marrow attenuation that can be associated with bone lesions. Additionally, axial color-coded imaging of the region of interest was performed using the bone marrow settings of the VNCa algorithm to help identify the target lesion. The optimal needle pathway was narrowed to a specific region based on analysis of the color map imaging. In some instances, there may be a few scattered areas of altered intramedullary color coding on a particular DECT image, and it may be difficult to determine whether a particular region represented tumor or hematopoietic marrow. However, the site of biopsy was chosen to correspond to the region of abnormal color-coding on DECT imaging that also corresponded most closely with the original PET or MRI finding. Core bone biopsies were performed co-axially using an 11-gauge Arrow OnControl Powered Bone Access System (Teleflex, Morrisville, NC, USA). As per our institutional routine, CT-guided bone biopsies were performed with intravenous moderate sedation administered by Interventional Radiology nurses and continuous monitoring throughout the procedure. At the completion of the procedure the patient was observed in the Interventional Radiology recovery area for 1 h to ensure that they were not experiencing any postprocedural complications.

As the biopsy needle was advanced to the surface of the bone, intermittent localizing axial CT was performed to confirm needle location and direction. CT technique

was switched to a routine monoenergetic setting (120 kV, 100 mAs, rotation time 0.5 s, pitch 0.5, 192×0.6 collimator) to reduce radiation dose (CTDI 6.7 mGy). As the needle was advanced to the edge of the lesion, DECT was again performed to determine whether the lesion could be seen outside of the pathway of the needle, which would necessitate redirection of the needle. In each case, the biopsy needle produced beam-hardening artifact, which was represented by a linear black band oriented along the long axis of the needle extending from the needle tip along the expected pathway of the biopsy. Although the artifact obscured the target lesion, it was useful to direct the needle toward the lesion as the needle was advanced. The needle was then advanced into the lesion, yielding between two and four specimens, which were analyzed by an on-site cytopathologist to confirm lesional material on initial touch prep analysis. The specimens were then sent to surgical pathology for frozen section to confirm the diagnosis and for final analysis. Finally, as significant metal artifact related to the biopsy needle was encountered on the intra-procedural images, a final DECT with bone marrow settings was obtained after the needle was removed to confirm that the needle tract intersected the lesion in question.

Results

Case 1

An 84-year-old man with a history of both prostate carcinoma and follicular lymphoma was thought to be in remission for both malignancies with an undetectable serum prostate-specific antigen (PSA). However, on surveillance PET/CT, the patient was found to have a new hypermetabolic focus in the posterior left iliac wing, and the SUV_{max} was measured at 4.3 (Fig. 1a). No definitive corresponding lesion was identified on the accompanying attenuation-corrected CT (Fig. 1b). Biopsy of the lesion was needed to differentiate prostatic metastasis from lymphomatous recurrence. Pre-procedural DECT color map images performed 2 weeks after the PET/CT identified a wedge-shaped area of green color thought to correspond to the lesion, on a background of purple bone marrow (Fig. 1c, d). Biopsy was performed with three passes over 50 min as described above (Fig. 1e), with pathology yielding “fragmented bone with an extensive lymphoid infiltrate consisting predominantly of small to medium-sized lymphocytes,” indicating follicular lymphoma, and not prostate cancer. Although we provided solid core bone fragments, flow cytometry of one of the biopsy samples was also performed,

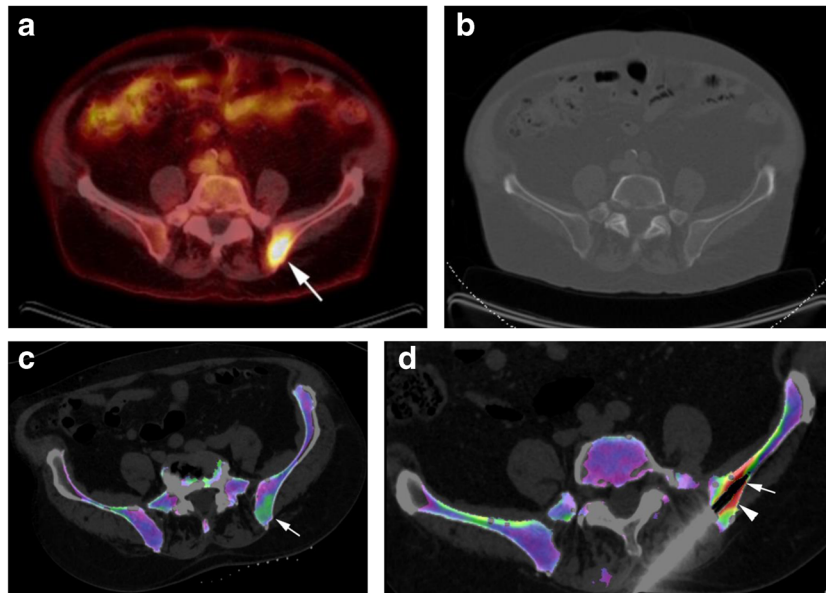


Fig. 1 Follicular lymphoma in a patient with a history of both prostate carcinoma and lymphoma. **a** Axial fused FDG-PET/CT image of the pelvis demonstrates a hypermetabolic focus in the posterior left iliac wing (*arrow*) that was not seen on previous imaging (not shown). **b** The attenuation correction CT of the pelvis from the same study failed to show an osseous lesion corresponding to the PET finding. DECT with bone marrow color mapping was then performed in an attempt to identify the lesion of concern before biopsy to better plan the biopsy tract. According to this color scale, normal marrow is generally coded in shades of blue and purple, whereas marrow lesions exhibit greener colors. **c** Initial large field-of-view (FOV) axial DECT pelvic color map image of the bone marrow reveals a suspicious focus corresponding to the

PET/CT abnormality (*arrow*). **d** Axial DECT color map after the biopsy needle was advanced to the surface of the bone shows significant distortion of the color coding with areas of beam-hardening artifact along the axis of the needle (*arrow*) and new artifactual orange and red shades (*arrowhead*) that obscure the region of interest. Importantly, this artifact is much less pronounced on images above and below the needle, and there were no signs that the lesion was located either cranial or caudal to the needle tip (not shown). The selected image is slightly cranial to the initial pre-procedure color map image as the biopsy needle penetrated the skin cranial to the lesion and the trajectory was caudally angulated to enter the region of concern. Histological assessment of the biopsy specimens confirmed the presence of follicular lymphoma in this region

which confirmed the diagnosis of B cell malignancy. As a result of the biopsy the patient started chemotherapy to treat follicular lymphoma.

Case 2

A 67-year-old man with a history of T3b prostate carcinoma with a Gleason score of 7 was status post-prostatectomy. The patient's serum PSA measured 0.76 at the time of imaging, and clinically, the patient was felt to be at a very low risk for metastatic disease. A routine follow-up prostate MRI showed an 11-mm, subtly enhancing lesion in the posterior left iliac wing (Fig. 2a). A subsequent monoenergetic CT of the pelvis was performed to confirm the lesion and help localize it before CT-guided biopsy (not shown). However, no correlate was visible on the CT images, and the patient was referred for DECT-guided biopsy. Pre-procedural DECT grayscale imaging shows a faint lucency in the posterior left iliac wing that was indeterminate, but may represent the lesion seen on MRI (Fig. 2b). The lucency measured 32 Hounsfield units, which was felt to be indeterminate for distinguishing a true soft-tissue lesion from either focal yellow marrow or localized osteoporosis given its size and intraosseous location. DECT color map images showed a 13-mm ovoid area of green color thought to correspond to the lesion depicted on MRI, on a background of purple marrow (Fig. 2c). Biopsy of the lesion was performed with four passes performed over 65 min to

confirm metastatic disease (Fig. 2d). The biopsy specimen was reported as: “bone fragments with blood and cellular marrow components involved in malignant glandular proliferation composed of small tightly packed glands with cells displaying high nuclear/cytoplasmic ratios, nuclear hyperchromasia, and eosinophilic cytoplasm.” Immunohistochemistry analysis of the biopsy samples was negative for PSA, but positive for NKX3.1 protein, which is seen in most prostate carcinomas and felt to be a specific and sensitive marker of prostate carcinoma. The lack of PSA staining on the core bone samples may explain why the patient's serum PSA remained low in the setting of osseous metastases. Thus, the biopsy confirmed the presence of metastatic disease and the patient was started on a chemotherapy regimen including hormone therapy.

Case 3

A 70-year-old woman with acute myelogenous leukemia was thought to be in relapse. Pelvic MRI was performed for tumor staging and demonstrated several subcentimeter, STIR-hyperintense, enhancing lesions in the iliac bones (Fig. 3a). The patient was referred for initial CT-guided bone biopsy. The monoenergetic CT of the pelvis did not demonstrate a corresponding abnormality (Fig. 3b, c) and the preprocedural MRI was used to plan biopsy needle trajectory as part of a routine CT-guided biopsy. However, no lesional material was detected on histological analysis (Fig. 3d). As a result, the patient was

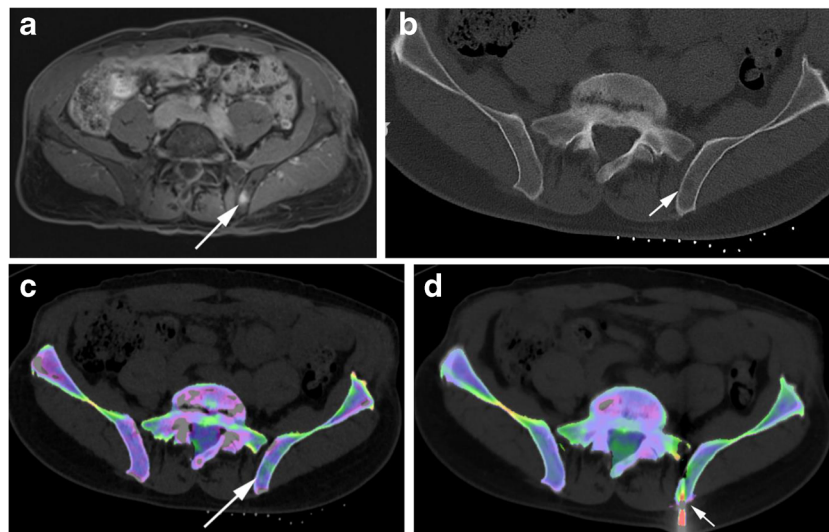


Fig. 2 Prostate carcinoma in a patient who was status post-prostatectomy and felt to be at a very low risk for metastatic disease. **a** Axial T1 spin echo fat-suppressed post-contrast image of the pelvis demonstrates an enhancing 11-mm lesion in the posterior left iliac wing (*arrow*). **b** Subsequent routine axial CT of the pelvis just before the biopsy does not show a convincing lesion, although there may be a faint oval region of decreased attenuation in the region of concern (*arrow*), which could represent a lesion or possibly an island of yellow marrow with trabecular rarefaction. **c** Color map imaging from a DECT performed with a bone marrow setting just before the biopsy reveals a faint area of green

corresponding to the enhancing lesion on MRI and the lucent lesion on the pre-biopsy CT images, which is not seen elsewhere in the posterior left ilium (*arrow*). The intensity of the green color is focally decreased in the area of the suspected lesion compared with other cases in this study, which probably reflects the focus of decreased attenuation on the grayscale image that was fused with the color map. **d** Color map DECT image during the biopsy demonstrates the needle pathway targeting the lesion detected on the pre-biopsy DECT color map images (*arrow*). Biopsy confirmed metastatic prostate carcinoma

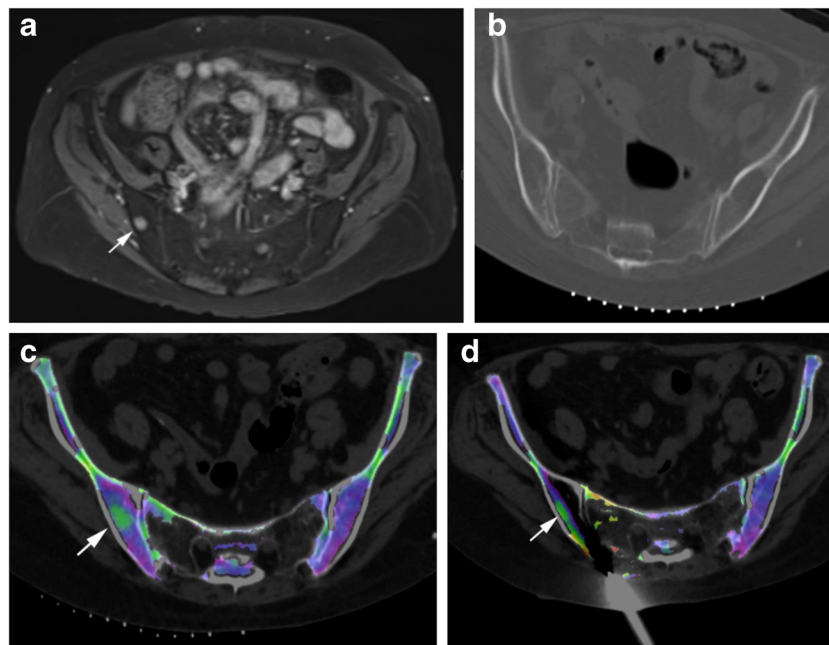


Fig. 3 Acute myeloid leukemia. **a** Axial T1 spin echo fat-suppressed post-contrast image of the pelvis shows a 1.2-cm enhancing lesion in the posterior right iliac wing (*arrow*) that was new compared with previous studies (not shown). An initial bone biopsy was unsuccessfully attempted using anatomical landmarks from the MRI. **b** An axial CT image viewed in bone windows from the initial biopsy does not show the target lesion either, and no lesional cells were identified at pathology. As a result, the patient was referred for repeat biopsy with DECT guidance. **c** Axial pelvic DECT color mapping just before needle

placement clearly demonstrates the lesion of concern (*arrow*). In this case, the 3D imaging was helpful in spatially localizing the lesion; however, the lesion was more conspicuous on the 2D axial images. **d** An axial pelvic DECT color map image with the needle on the surface of the posterior iliac wing directed toward the lesion shows significant beam-hardening artifact that obscures the underlying bone and much of the lesion (*arrow*). However, the orientation of the artifact indicates the biopsy tract and can be helpful in directing needle advancement. The final pathology report yielded acute myeloid leukemia

referred for DECT-guided iliac bone biopsy to confirm metastatic disease. Pre-procedural DECT color map images showed a 16-mm ovoid area of green color on a background of purple bone marrow (Fig. 3e, f), presumably corresponding to the 9-mm lesion demonstrated on MRI. Biopsy of the lesion was performed with four passes performed over 45 min (Fig. 3g) and samples reviewed by pathology yielded: “multiple large sheets of immature monocytic cells most consistent with acute myeloid leukemia with monocytic differentiation.” Immunophenotypic analysis differed from the patient’s previous bone marrow studies, which further guided therapeutic management.

Case 4

A 66-year-old female patient with a history of breast carcinoma was thought to be in remission and developed new-onset low back pain. However, given the patient’s history, MRI with contrast medium administration followed by whole-body bone scintigraphy were obtained to evaluate the cause of the patient’s symptoms, including possible osseous metastatic disease. There were several areas of increased radiotracer uptake on nuclear medicine bone scan (not shown) and an enhancing 5-mm lesion in the posterior left iliac wing identified on MRI (Fig. 4a); however, only a single lesion located at the right

femoral head/neck junction was identified on staging CT chest/abdomen/pelvis (Fig. 4b, c). The authors believed that the posterior left iliac wing lesion was technically easier and safer to biopsy than other lesions, and DECT was used to localize and biopsy the lesion. Pre-procedural DECT color map images showed a 7-mm green rounded focus on a background of purple marrow, which was felt to correspond to the lesion demonstrated on MRI (Fig. 4d, e). Biopsy of the lesion was performed with two passes performed over 45 min (Fig. 4f, g). Histological analysis of the biopsy specimens resulted in “fragments of mature bone involved in malignant proliferation of cells in small clusters with enlarged round to oval hyperchromatic nuclei with high nuclear/cytoplasmic ratio and scant eosinophilic cytoplasm,” diagnostic of metastatic breast carcinoma. Immunohistochemistry showed that the lesion was estrogen receptor-positive, but progesterone receptor- and HER-2/neu-negative.

Discussion

Bone marrow assessment on DECT is increasingly becoming part of routine clinical practice, and has been reported to help improve detection and characterization of traumatic,

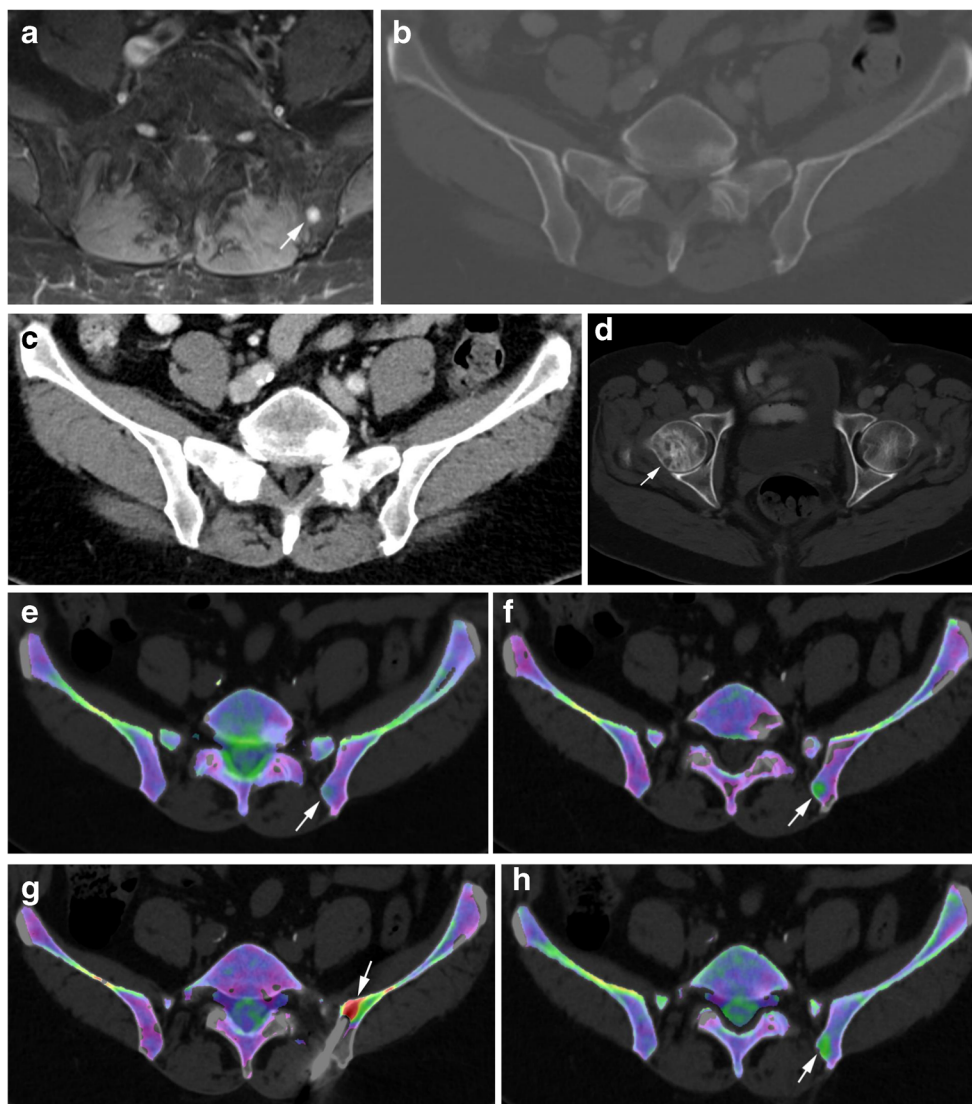


Fig. 4 Breast carcinoma and new onset of low back pain. **a** Axial T1 spin echo fat-suppressed post-contrast image of the lower lumbar spine reveals a 0.9-cm posterior left iliac wing lesion (*arrow*) suspicious for a metastasis. Axial CT of the pelvis viewed in **b** bone and **c** a soft-tissue windows does not show a lesion in this area, and the patient was scheduled for a DECT-guided biopsy of the lesion. **d** Axial CT image of the abdomen and pelvis performed 2 weeks before the biopsy demonstrated a primarily sclerotic focus in the right femoral head (*arrow*) that extended to the femoral head/neck junction. This was a deeper lesion that was surrounded by muscle and neurovascular structures. The posterior iliac lesion was more superficial and not deep to major neurovascular structures. As a result, this was selected for initial biopsy. **e** Just before biopsy, an initial axial DECT with bone marrow

color mapping was performed with a 3-mm slice thickness. There is a faint area of green color (*arrow*) corresponding to the area of interest that could represent the target lesion. However, this is similar to shades of green marrow color elsewhere in the pelvis. **f** The scan was repeated after decreasing the slice thickness to 1.5 mm and the lesion of interest is now clearly visible (*arrow*). **g** Repeat DECT after advancing the needle shows the needle positioned in the expected area of the lesion with significant distortion of the color map (*arrow*). **h** Nearly all of the color-coding distortion resolves after removal of the needle, suggesting that the device might make a large contribution to the color map alteration, although the residual color map abnormality is slightly larger (*arrow*) than the original lesion on the pre-biopsy image. The final diagnosis was metastatic breast carcinoma

rheumatological, and neoplastic processes that affect the marrow. The linear attenuation coefficient is a fundamental parameter of both monoenergetic and dual-energy CT. It discriminates tissues in the imaging plane based on their ability to stop X-rays from reaching the imaging detector, in turn creating an image of contrasting shades of black, gray, and white. This enables the delineation of different structures or pathological conditions from one another, such as a “gray”

fracture line within a “white” bone. The mass density and composition of a particular material, in addition to how photons interact with the material, are the primary parameters that define the linear attenuation coefficient. Monoenergetic CT primarily exploits differences in mass density, whereas DECT uses differences in both mass density and material composition. Therefore, two objects with the same mass density, but different material compositions may appear identical

at a certain energy level on a monoenergetic CT, but can be seen as two distinct structures by varying the X-ray energy with DECT [43–45].

Monoenergetic CT is the primary modality utilized for bone lesion biopsy given its relative availability and ability to easily and rapidly identify most bone lesions, which are either sclerotic (denser than the adjacent bone) or lucent (less dense than the adjacent bone). However, when a lesion has a mass density that is nearly identical to the adjacent bone, monoenergetic CT is unable to depict the lesion, and the radiologist must rely heavily on anatomical landmarks when planning the needle trajectory for percutaneous biopsy [29]. This technical approach increases the risk for sampling error, potentially necessitating repeat biopsy, which in turn increases costs, often delays treatment, and may increase the patient's anxiety level while awaiting a definitive diagnosis. Therefore, when a lesion demonstrated on MRI, nuclear bone scintigraphy, or PET/CT is isodense or nearly isodense to adjacent bone on monoenergetic CT, DECT can use differences in material composition to assign the lesion a different color or shade of gray than the adjacent bone on the image display. The interventionalist may then more accurately plan the biopsy trajectory to the area of interest, decreasing sampling error, and thus decreasing costs and delays in treatment.

We present a novel approach to using DECT to help refine the biopsy trajectory for lesions that are readily apparent on MRI or PET/CT, but where either no definitive correlate is identified on monoenergetic CT or the target is faint and there is potential for sampling error. A series of four patients with varying malignancies, including prostate carcinoma, lymphoma, acute myelogenous leukemia, and breast carcinoma, all underwent biopsy of an iliac bone lesion. Pre-procedural color maps were the primary method used to identify an appropriate biopsy tract through which the needle would advance to access the lesion. Comparison of the color maps with the initial pre-procedural imaging demonstrating the target lesion, either MRI or PET/CT, was performed to confirm that the appropriate region was selected for biopsy. After initial entry of the needle, color map images were again employed, depicting linear beam-hardening artifact that obscured the lesion in question along with significant distortion of the color coding. Although this artifact could potentially prevent accurate needle advancement into the target lesion, we found that the linear beam hardening artifact was useful to confirm the accurate trajectory of the needle. Following removal of the needle, the color map images demonstrated that the color map distortion almost completely resolved, suggesting that this distortion might have been almost entirely related to the presence of the metal rather than the biopsy technique. All of the biopsy specimens yielded lesional tissue, which indicates that there was no significant sampling error. Malignant cells were identified by the

pathologist in each case at the time of biopsy and the final pathology results were available a few days after biopsy and helped guide therapeutic management for each patient.

Although one patient only had a preprocedural PET/CT demonstrating the lesion, which precluded accurate size measurements, it should be noted that three of our four patients had preprocedural MRIs that demonstrated target lesions measuring less than 1.5 cm in their greatest dimension. Several authors have reported significantly lower diagnostic yield and accuracy when biopsying smaller lesions, particularly when they were smaller than 2 cm [23, 46]. Our case series demonstrates that directly visualizing small target lesions during DECT-guided bone biopsies may potentially help to increase diagnostic yield. Of note, in the 3 cases in which there was a pre-procedural MRI, the measured size of the target lesion was slightly larger on the DECT color-coded images than on the MRI. Although we attempted to biopsy the center of each target lesion it may be interesting to determine on additional cases whether this difference in measured size could lead to sampling error if the periphery of the lesion on the DECT color maps was sampled rather than the center.

In two patients, we noted that the target lesions were either not visible or difficult to discern from background marrow on DECT bone marrow color maps when the images were acquired using a larger slice thickness (3 mm). These lesions became more conspicuous when using a thinner slice thickness (1.5 mm). Our first patient (case 1) took more than 1 h between the start of the first DECT scan and removal of the biopsy needle. This was primarily because we obtained DECT imaging and performed post-processing of the VNCa bone marrow setting several times before, during, and after the procedure to optimize our imaging and procedural technique. This included selecting the optimal CT slice thickness and best color map settings to display the target lesion in addition to the biopsy needle. In addition, we took several passes through the lesion to increase diagnostic yield. However, as we became more comfortable with this technique and optimized the imaging parameters, we were able to reduce the procedure time to less than 1 h, which is only slightly greater than our usual bone biopsy times when lesions are clearly visible on monoenergetic CT imaging. The standard of care at our institution is to involve a cytopathologist during biopsies of lytic and isodense bone lesions to confirm that the tissue samples contain lesional material. Although this lengthens procedure times, it has reduced the number of repeat biopsies we have had for insufficient material [47].

Several limitations to our series exist, most notably the small sample size of four patients. The patients were not selected for type of malignancy, and it is unclear whether certain bone tumors, such as those from solid tumor metastases, are more discernable on DECT than hematological malignancies, such as lymphoma or multiple myeloma. Correlation with FDG avidity on PET was also not considered, and it is possible

that only lesions with significantly elevated SUV values may be more identifiable on the DECT color map images. All of these lesions were located in the iliac bones, though presumably the same DECT parameters would apply to lesions in other areas. Furthermore, anatomical landmarks from preprocedural imaging studies have long been used with varying success to guide biopsy of isodense bone lesions and this approach may have achieved the same results as those obtained following DECT biopsy. We did not encounter a lesion that was detected on MRI or PET, but imperceptible on the DECT color-coded images. It is certainly possible that some lesions referred for this technique may not be visible on the DECT color maps. In these cases, we would rely on the preprocedural MRI or PET to provide a road map to guide the appropriate needle trajectory. Future work may be centered around these and other issues, including comparing DECT with MRI-guided bone lesion biopsy, and quantifying the difference in radiation dose between monoenergetic CT and DECT using a larger sample size. Finally, artifact related to the biopsy needle could potentially obscure the target lesion and result in the selection of a suboptimal needle pathway. Further studies could be performed to determine whether the concurrent use of iterative metal artifact reduction techniques that are currently clinically available could be helpful in reducing the artifact and allowing better visualization of the lesion as the needle is advanced.

In conclusion, DECT using the bone marrow setting may be helpful in directly visualizing osseous lesions that are occult on monoenergetic CT and directing CT-guided percutaneous biopsies of these lesions.

Compliance with ethical standards

Conflicts of interest The authors declare that they have no conflicts of interest.

References

1. Glazebrook KN, Guimaraes LS, Murthy NS, et al. Identification of intraarticular and periarticular uric acid crystals with dual-energy CT: initial evaluation. *Radiology*. 2011;261(2):516–24.
2. Nicolaou S, Liang T, Murphy DT, Korzan JR, Ouellette H, Munk P. Dual-energy CT: a promising new technique for assessment of the musculoskeletal system. *AJR Am J Roentgenol*. 2012;199(5 Suppl):S78–86.
3. Deng K, Zhang CQ, Li W, et al. Preliminary application of high-definition CT gemstone spectral imaging in hand and foot tendons. *Korean J Radiol*. 2012;13(6):743–51.
4. Glazebrook KN, Brewerton LJ, Leng S, et al. Case-control study to estimate the performance of dual-energy computed tomography for anterior cruciate ligament tears in patients with history of knee trauma. *Skeletal Radiol*. 2014;43(3):297–305.
5. Coupal TM, Mallinson PI, McLaughlin P, Nicolaou S, Munk PL, Ouellette H. Peering through the glare: using dual-energy CT to overcome the problem of metal artefacts in bone radiology. *Skeletal Radiol*. 2014;43(5):567–75.
6. Reddy T, McLaughlin PD, Mallinson PI, et al. Detection of occult, undisplaced hip fractures with a dual-energy CT algorithm targeted to detection of bone marrow edema. *Emerg Radiol*. 2015;22(1):25–9.
7. Gondim Teixeira PA, Gervaise A, Louis M, et al. Musculoskeletal wide detector CT: principles, techniques and applications in clinical practice and research. *Eur J Radiol*. 2015;84(5):892–900.
8. Sun X, Shao X, Chen H. The value of energy spectral CT in the differential diagnosis between benign and malignant soft tissue masses of the musculoskeletal system. *Eur J Radiol*. 2015;84(6):1105–8.
9. Mallinson PI, Coupal TM, McLaughlin PD, Nicolaou S, Munk PL, Ouellette HA. Dual-energy CT for the musculoskeletal system. *Radiology*. 2016;281(3):690–707.
10. Burke CJ, Didolkar MM, Barnhart HX, Vinson EN. The use of routine non density calibrated clinical computed tomography data as a potentially useful screening tool for identifying patients with osteoporosis. *Clin Cases Miner Bone Metab*. 2016;13(2):135–40.
11. Diekhoff T, Hermann KG, Pumberger M, Hamm B, Putzier M, Fuchs M. Dual-energy CT virtual non-calcium technique for detection of bone marrow edema in patients with vertebral fractures: a prospective feasibility study on a single-source volume CT scanner. *Eur J Radiol*. 2017;87:59–65.
12. Hackenbroch C, Riesner HJ, Lang P, et al. Dual energy computed tomography in musculoskeletal imaging, with focus on fragility fractures of the pelvis. *Z Orthop Unfall*. 2017;155(6):708–15.
13. Khanduri S, Goyal A, Singh B, et al. The utility of dual energy computed tomography in musculoskeletal imaging. *J Clin Imaging Sci*. 2017;7:34.
14. Thomas C, Schabel C, Krauss B, et al. Dual-energy CT: virtual calcium subtraction for assessment of bone marrow involvement of the spine in multiple myeloma. *AJR Am J Roentgenol*. 2015;204(3):W324–31.
15. Chang JJ, Ilaşlan H, Sundaram M, Schils J, Subhas N. CT-guided percutaneous biopsy of sclerotic bone lesions: diagnostic outcomes. *Skeletal Radiol*. 2018;47(5):661–9.
16. Espinosa LA, Jamadar DA, Jacobson JA, et al. CT-guided biopsy of bone: a radiologist's perspective. *AJR Am J Roentgenol*. 2008;190(5):W283–9.
17. Rehm J, Veith S, Akbar M, Kauczor HU, Weber MA. CT-guided percutaneous spine biopsy in suspected infection or malignancy: a study of 214 patients. *Rofo*. 2016;188(12):1156–62.
18. Song Y, Kwon JW. Percutaneous CT-guided sternal biopsy: factors affecting the diagnostic yield. *Acta Radiol*. 2017;58(7):825–33.
19. Cox M, Pukenas B, Poplawski M, Bress A, Deely D, Flanders A. CT-guided cervical bone biopsy in 43 patients: diagnostic yield and safety at two large tertiary care hospitals. *Acad Radiol*. 2016;23(11):1372–5.
20. Garg V, Kosmas C, Josan ES, et al. Computed tomography-guided percutaneous biopsy for vertebral neoplasms: a department's experience and hybrid biopsy technique to improve yield. *Neurosurg Focus*. 2016;41(2):E17.
21. Chang CY, Huang AJ, Bredella MA, et al. Percutaneous CT-guided needle biopsies of musculoskeletal tumors: a 5-year analysis of non-diagnostic biopsies. *Skeletal Radiol*. 2015;44(12):1795–803.
22. Maciel MJ, Tyng CJ, Barbosa PN, et al. Computed tomography-guided percutaneous biopsy of bone lesions: rate of diagnostic success and complications. *Radiol Bras*. 2014;47(5):269–74.
23. Li Y, Du Y, Luo TY, et al. Factors influencing diagnostic yield of CT-guided percutaneous core needle biopsy for bone lesions. *Clin Radiol*. 2014;69(1):e43–7.
24. Kaltsikis I, Chourmouzi D, Drevelegas K, Potsi S, Moutmzouoglou A, Drevelegas A. Core needle biopsy of spinal lesions under CT guidance: review of 79 cases. *J Neurol Surg A Cent Eur Neurosurg*. 2012;73(4):199–203.
25. Hwang S, Lefkowitz RA, Landa J, et al. Percutaneous CT-guided bone biopsy: diagnosis of malignancy in lesions with initially

- indeterminate biopsy results and CT features associated with diagnostic or indeterminate results. *AJR Am J Roentgenol.* 2011;197(6):1417–25.
26. Omura MC, Motamedi K, UyBico S, Nelson SD, Seeger LL. Revisiting CT-guided percutaneous core needle biopsy of musculoskeletal lesions: contributors to biopsy success. *AJR Am J Roentgenol.* 2011;197(2):457–61.
 27. Rimondi E, Rossi G, Bartalena T, et al. Percutaneous CT-guided biopsy of the musculoskeletal system: results of 2027 cases. *Eur J Radiol.* 2011;77(1):34–42.
 28. Rimondi E, Staals EL, Errani C, et al. Percutaneous CT-guided biopsy of the spine: results of 430 biopsies. *Eur Spine J.* 2008;17(7):975–81.
 29. Hillen TJ, Talbert RJ, Friedman MV, et al. Biopsy of CT-occult bone lesions using anatomic landmarks for CT guidance. *AJR Am J Roentgenol.* 2017;209(1):214–21.
 30. Sequeiros RB, Fritz J, Ojala R, Carrino JA. Percutaneous magnetic resonance imaging-guided bone tumor management and magnetic resonance imaging-guided bone therapy. *Top Magn Reson Imaging.* 2011;22(4):171–7.
 31. Carrino JA, Khurana B, Ready JE, Silverman SG, Winalski CS. Magnetic resonance imaging-guided percutaneous biopsy of musculoskeletal lesions. *J Bone Joint Surg Am.* 2007;89(10):2179–87.
 32. Guo W, Hao B, Chen HJ, et al. PET/CT-guided percutaneous biopsy of FDG-avid metastatic bone lesions in patients with advanced lung cancer: a safe and effective technique. *Eur J Nucl Med Mol Imaging.* 2017;44(1):25–32.
 33. Cornelis F, Silk M, Schoder H, et al. Performance of intra-procedural 18-fluorodeoxyglucose PET/CT-guided biopsies for lesions suspected of malignancy but poorly visualized with other modalities. *Eur J Nucl Med Mol Imaging.* 2014;41(12):2265–72.
 34. Palmer WE, Simeone FJ. Can dual-energy CT challenge MR imaging in the diagnosis of focal infiltrative bone marrow lesions? *Radiology.* 2018;286(1):214–6.
 35. Kosmala A, Weng AM, Krauss B, Knop S, Bley TA, Petritsch B. Dual-energy CT of the bone marrow in multiple myeloma: diagnostic accuracy for quantitative differentiation of infiltration patterns. *Eur Radiol.* 2018. <https://doi.org/10.1007/s00330-018-5537-5>.
 36. Kosmala A, Weng AM, Heidemeier A, et al. Multiple myeloma and dual-energy CT: diagnostic accuracy of virtual noncalcium technique for detection of bone marrow infiltration of the spine and pelvis. *Radiology.* 2018;286(1):205–13.
 37. Yuan Y, Zhang Y, Lang N, Li J, Yuan H. Differentiating malignant vertebral tumours from non-malignancies with CT spectral imaging: a preliminary study. *Eur Radiol.* 2015;25(10):2945–50.
 38. Dong Y, Zheng S, Machida H, et al. Differential diagnosis of osteoblastic metastases from bone islands in patients with lung cancer by single-source dual-energy CT: advantages of spectral CT imaging. *Eur J Radiol.* 2015;84(5):901–7.
 39. Chen H, Jia M, Xu W. Malignant bone tumor intramedullary invasion: evaluation with dual-energy computed tomography in a rabbit model. *J Comput Assist Tomogr.* 2015;39(1):70–4.
 40. Zheng S, Dong Y, Miao Y, et al. Differentiation of osteolytic metastases and Schmorl's nodes in cancer patients using dual-energy CT: advantage of spectral CT imaging. *Eur J Radiol.* 2014;83(7):1216–21.
 41. Lee YH, Kim S, Lim D, Suh JS, Song HT. Spectral parametric segmentation of contrast-enhanced dual-energy CT to detect bone metastasis: feasibility sensitivity study using whole-body bone scintigraphy. *Acta Radiol.* 2015;56(4):458–64.
 42. Crone-Münzebrock W, Carl UM. Dual-energy CT-scan quantification of recalcification in osteolyses of the vertebral body due to mammary carcinomas in the course of antineoplastic treatment. *Clin Exp Metastasis.* 1990;8(2):173–9.
 43. McCollough CH, Leng S, Yu L, Fletcher JG. Dual- and multi-energy CT: principles, technical approaches, and clinical applications. *Radiology.* 2015;276(3):637–53.
 44. Omoumi P, Becce F, Racine D, Ott JG, Andreisek G, Verdun FR. Dual-energy CT: basic principles, technical approaches, and applications in musculoskeletal imaging I. *Semin Musculoskelet Radiol.* 2015;19(5):431–7.
 45. Omoumi P, Verdun FR, Guggenberger R, Andreisek G, Becce F. Dual-energy CT: basic principles, technical approaches, and applications in musculoskeletal imaging II. *Semin Musculoskelet Radiol.* 2015;19(5):438–45.
 46. Wu JS, Goldsmith JD, Horwich PJ, Shetty SK, Hochman MG. Bone and soft-tissue lesions: what factors affect diagnostic yield of image-guided core-needle biopsy? *Radiology.* 2008;248(3):962–70.
 47. Virayavanich W, Ringler MD, Chin CT, et al. CT-guided biopsy of bone and soft-tissue lesions: role of on-site immediate cytologic evaluation. *J Vasc Interv Radiol.* 2011;22(7):1024–30.